SLAC-PUB-15439

Titanium d_{xy} ferromagnetism at the $LaAlO_3/SrTiO_3$ interface

J.-S. Lee[1,*], Y. W. Xie[2], H. K. Sato[3], C. Bell[3], Y. Hikita[3], H. Y. Hwang[2,3], C.-C. Kao[1]

[1]*Stanford Synchrotron Radiation Lightsource, SLAC National Accelerator Laboratory, Menlo Park, California 94025, USA*

[2]*Geballe Laboratory for Advanced Materials, Department of Applied Physics, Stanford University, Stanford, California 94305, USA*

[3]*Stanford Institute for Materials and Energy Sciences, SLAC National Accelerator Laboratory, Menlo Park, California 94025, USA*

* email: jslee@slac.stanford.edu (J.L)

A number of recent transport and magnetization studies have shown signs of ferromagnetism in the $LaAlO_3/SrTiO_3$ heterostructure[1-6], an unexpected property with no bulk analog in the constituent materials. However, no experiment thus far has provided direct information on the host of the magnetism[7-11]. Here we report spectroscopic investigations of the magnetism using element-specific techniques, including x-ray magnetic circular dichroism and x-ray absorption spectroscopy, along with corresponding model calculations. We find direct evidence for in-plane ferromagnetic order at the interface, with Ti^{3+} character in the d_{xy} orbital of the anisotropic t_{2g} band. These findings establish a striking example of emergent phenomena at oxide interfaces.

Recent advances in the atomic-scale synthesis and characterization of perovskite oxide heterostructures have engendered significant interest in their electronic and magnetic structure.

Division of Materials Sciences and Engineering, under contract DE-AC02-76SF00515 and BES.

Given their vast physical properties in bulk form, and their epitaxial compatibility, perovskites provide an ideal arena to explore the competition, interaction, and creation of many ground states at their interfaces[12]. The $LaAlO_3/SrTiO_3$ heterostructure is a canonical example, exhibiting interface conductivity[13], superconductivity[14], and ferromagnetism[1-6] at the interface between two wide band-gap insulators. From a fundamental perspective, ferromagnetism is perhaps the most important property; although bulk $SrTiO_3$ can be doped to be metallic and superconducting, neither constituent in bulk form exhibits ferromagnetism. Hence interface ferromagnetism here could be a leading example of truly emergent phenomena. Most previous studies used bulk probes (macroscopic magnetization or torque)[3, 4]; while scanning SQUID microscopy could localize the magnetism to the near surface region[5, 15], the specific location where the moments reside is beyond the resolution of the probe. In principle, magnetism could arise from cation/anion defects in the $LaAlO_3$ or $SrTiO_3$, or could be specific to the interface; theoretical scenarios have been proposed for all of these mechanisms[7-11]. Thus it is of central importance to determine the microscopic nature of the observed ferromagnetism.

To address this issue, we applied element-specific techniques at the $LaAlO_3/SrTiO_3$ (001) interface, namely synchrotron radiation based x-ray absorption spectroscopy (XAS) and x-ray magnetic circular dichroism (XMCD) (see Materials and Methods section). These measurements can uniquely determine whether the observed magnetization is due to a magnetic moment ($\vec{M}$) from one of the constituent elements, or from extrinsic impurities. All spectra were acquired by recording the total electron yield (TEY). Since the maximum probing depth of TEY is approximately 5~10 nm, these measurements are very sensitive to the interface with proper choice of $LaAlO_3$ thickness. Using the angle dependence of the XMCD signal, which is proportional to $\vec{K} \cdot \vec{M}$ (where $\vec{K}$ is the x-ray propagation vector), we can also determine the

direction of the magnetic moment. Moreover, due to the high sensitivity of XMCD[16], a very small magnetic moment (~0.005 μ_B/atom) can be detected. For this work, $LaAlO_3/SrTiO_3$ (hereafter LAO/STO) heterostructures with differing numbers of LAO unit cells (UC) were grown by pulsed laser deposition (see Materials and Methods section). XAS measurements were used to check for the possibility of magnetic impurities; *e.g.* typical magnetic 3*d*-transition metals, Cr, Mn, Fe, Co, and Ni (see Supplementary Information); none were observed down to our resolution limit (~10^{12} atoms/cm^2)[16].

In the absence of extrinsic magnetic impurities, interface ferromagnetism is perhaps most likely to originate from Ti atoms[8-11]. Therefore we performed Ti $L_{2,3}$-edges XMCD measurements LAO(1, 2, 3.3, and 10 UC)/STO, as well as bare STO crystals, at temperature T = 10 K. The experimental geometry is shown in Fig. 1a, where θ is the angle between $\vec{M}$ and $\vec{K}$. θ was set at 30^o (90^o) to optimize the observation of an in-plane (out-of-plane) magnetic moment. With the 30^o geometry, a Ti XMCD signal on 3.3 UC is clearly seen (Fig. 1b), although the dichroism ($\Delta\rho$) is very weak. Note that the 10 UC sample was confirmed to exhibit a comparable XMCD response. Furthermore, the Ti $\Delta\rho$ signal completely disappears at room temperature, as well as for $\theta = 90^o$ (Fig. 1c), indicating the ferromagnetic Ti moment is parallel to the film surface, which is also confirmed by the *M vs H* (hysteresis) curve that was obtained by monitoring the XMCD intensity at the Ti L_3-edge. For this in-plane configuration, $\Delta\rho$ is ~ 0.5% of the total absorption signal. The total magnetic moment can be estimated to be ~0.01 μ_B/Ti if we assume that the Ti moment is uniform within the probing volume of TEY mode, and ~ 0.1 μ_B/Ti if uniform magnetic Ti are confined to a single unit cell at the STO/LAO interface (see Supplementary Information). We note that the observed magnetic behavior via Ti XMCD is consistent with scanning SQUID studies of the same sample[15] when averaging the observed

inhomogeneous dipoles, and also consistent with the upper bound based on neutron reflectivity[17], although we note that the latter study was carried out on superlattice samples, which may possess different material characteristics to the single layer samples studied here. It should be noted that the ferromagnetic dipoles seen by scanning SQUID were limited to zero applied magnetic field. As a further control we also studied single crystal LAO, and single crystal STO substrates, as well as 1 UC and 2 UC LAO/STO heterostructures, all showing no XMCD signal, consistent with the critical LAO thickness for magnetism found by scanning SQUID[15].

The Ti XMCD suggests that within the probing volume of the sample, the Ti valence state is mixed, consistent with previous observations[18, 19], since the $3d^0$ configuration of Ti^{4+} in bulk STO cannot generate a ferromagnetic polarization at the 3*d*-band in and of itself. To confirm this point, atomic multiplet calculations[20, 21] were used to simulate XMCD spectra for the Ti^{3+} and Ti^{4+} states. The calculated Ti^{3+} XMCD spectrum agrees well with the experimental result (Fig. 1b).

Since the LAO thickness is thin, the TEY signal probes both the Ti just at the interface, and extending further into the substrate. To pinpoint the location of the polarized Ti^{3+} state as the origin of the $\Delta\rho$ signal, we performed XAS measurements (Fig. 2a) on a series of LAO/STO samples with varying thickness of LAO(1-25 UC), as well as bare STO. Considering the probing depth of the TEY signal, and the absence of Ti in the LAO layer, these measurements correspond to increasing the relative contribution from the LAO/STO interface with increasing LAO thickness (Fig. 2a inset). In particular, for thicker LAO samples (*i.e.* comparable to the TEY probing depth), the detected signal is dominated by the interfacial Ti.

These spectra were compared with multiplet calculations of pure $SrTiO_3$ (i.e., only Ti^{4+} valence) and pure $LaTiO_3$ (Ti^{3+}). The calculations show that the overall spectral features on Ti^{3+}

multiplet states move to lower photon energy compared with that of the Ti^{4+} feature. Using a 2-dimensional XAS map (LAO-thickness *vs.* photon energy, *E*), we examined spectral features around the Ti L_3-edge (Fig. 2b), which show intense lines at both E = 457.1 and 459.4 eV, corresponding to the Ti t_{2g} and e_g orbital levels, respectively. Similar features were found at the Ti L_2-edge (see Supplementary Information). With varying thickness of LAO, no change is observed in the e_g level. By contrast, the t_{2g} level shows an energy shift with increasing LAO thickness, for which the interfacial signal is enhanced. The t_{2g} level moves to lower photon energy, estimated to be ~ 40 meV (Fig. 2c). This result, in combination with the multiplet calculations, locates the magnetic Ti^{3+} state at the interface, with fractional occupancy of an additional electron state ($3d^1$) in the t_{2g} orbital band.

We now turn to discuss our model calculations of the XMCD spectra, for which a tetragonally distorted TiO_6 octahedron was employed, leading to an energy splitting for both the degenerate t_{2g} and e_g orbital bands. The existence of such a distorted structure is verified by Ti *L*-edges x-ray absorption linear dichroism (XLD) measurements of the LAO/STO heterostructure (see Supplementary Information). Excellent overall agreement between the in-plane XMCD experiment and simulation (Fig. 1b) is achieved by reducing the orbital degeneracy of the 3*d* Ti states. Indeed, we found that the energy of planar orbitals (d_{xy} and d_{x2-y2}) in both the t_{2g} and e_g bands is lower than that of the out-of-plane orbitals (Fig. 3a), in good agreement with previous studies of the orbital reconstruction[22-24]. Accordingly, the additional electron ($3d^1$) in the Ti^{3+} state occupies the polarized d_{xy} orbital level (Fig. 3a).

An independent confirmation of this interpretation of the *L*-edge spectra can be found by noting that orbitally-selective magnetic polarization should be present in the neighboring oxygen, due to O 2*p*-Ti 3*d* hybridization. Hence we performed XMCD measurements at the O *K*-edge,

and clearly observed a dichroism feature (Fig. 4a), which is pronounced only around E = 529.2 eV. This energy region corresponds to the oxygen bonding with the Ti t_{2g} band[22], whereas the e_g band feature is around E = 532.5 eV. Oxygen spin contributions in the XMCD measurement are cancelled out, because of the lack of spin-orbit coupling in the oxygen 1*s* shell. Thus the observed XMCD signal at the O *K*-edge originates from the projected Ti 3*d* orbital contributions. To resolve the specific orbital character that is magnetically bonding with oxygen, we measured XLD at the O *K*-edge (Fig. 4b). Using the variation of the XLD signal, the contribution of each orbital character can be assigned. In particular, the d_{xy} contribution is around E ~ 529 eV, just where the O *K*-edge dichroism is observed. These findings clearly support the prior conclusion that the ferromagnetic Ti at the interface is associated with the d_{xy} orbital in the t_{2g} band.

These O *K*-edge spectra are also useful for considering some of the defect-based theoretical scenarios which might be relevant for the LAO/STO heterostructure. For scenarios based on interfacial oxygen vacancies[10], we note that in general, the presence of oxygen defects tends to broaden all O *K*-edge XAS features due to the reduced lifetime in the resonant process, and disorder in the local coordination. Thus we measured the evolution of the O *K*-edge XAS from a series of samples with differing LAO thickness (Fig. 4c). For thicker (thinner) LAO, the spectrum is quite similar to that of bulk LAO (STO). However, the spectral changes in the region around 542.5 eV (i.e., La/Al/Ti-O bonding) suggest a reconstructed interface electronic structure that becomes pronounced above 3 UC, consistent with the reported critical thickness for conductivity, magnetism, and orbital splitting[15, 23, 25]. On the other hand, the absorption-widths at both the t_{2g} and e_g regions for all samples are nearly identical within our experimental resolution (see Supplementary Information). Ultimately, a clear delineation of the source of magnetism between Ti and oxygen fundamentally cannot be made, due to the O 2*p*-Ti 3*d* hybridization

discussed above. However, oxygen defects may play a role at a level below our detection threshold; the theoretical studies[10] were based on a relatively high concentration of defects, resulting in a correspondingly high Ti moment (~ 0.34 μ_B), much larger than observed here.

Materials and Methods

The $LaAlO_3(x)/SrTiO_3$ (001) samples were prepared by growing x UC of $LaAlO_3$ on commercial TiO_2-terminated (001) STO substrates by pulsed laser deposition[26]. The $LaAlO_3$ was deposited at 800^{o}C with an oxygen partial pressure of 10^{-5} mbar, after a pre-annealing at 950^{o}C with an oxygen partial pressure of 5×10^{-6} mbar for 30 min. The samples were cooled to 600^{o}C, and annealed in a high-pressure oxygen environment (0.4 bar) for one hour. The transport properties of these samples were nominally identical to those reported elsewhere[26, 27].

The XMCD spectra show white line resonances at the Ti $L_{2,3}$-edges. The spectra (ρ^+ and ρ^-) represent, respectively, the parallel and anti-parallel alignment of the magnetization direction with the photon helicity vector. ρ^+ and ρ^-, which result from Ti $2p \rightarrow 3d$ dipole transitions, are divided roughly into the L_3 ($2p_{3/2}$) and L_2 ($2p_{1/2}$) regions. The dichroism ($\Delta\rho = \rho^+ - \rho^-$) is the difference between the two spectra, and XAS is their summation ($\rho^+ + \rho^-$). We obtained the $\Delta\rho$ spectra by reversing the polarity (right- or left-circular) of the incident photon beam, and by changing the direction of the external magnetic (H = +/- 0.2 T) field at a fixed polarity. The degree of circular polarization was ~ 95%. For the LD measurements via XAS, the polarization direction of the linearly polarized x-rays (98% polarized) was tuned by rotating the x-ray incident angle, with 90^o and 30^o incident corresponding to complete in-plane ($E//a$) and majority

out-of-plane (*E*//*c*) polarized components, respectively. All spectroscopic experiments (XAS and XMCD) were carried out at beamlines BL 10-1 and 13-1 at the Stanford Synchrotron Radiation Lightsource (SSRL).

LIST OF REFERENCES

[1] Brinkman, A. *et al*. Magnetic effects at the interface between non-magnetic oxides. *Nature Mater.* **6**, 493-496 (2007).

[2] Dikin, D. A. *et al*. Coexistence of superconductivity and ferromagnetism in two dimensions. *Phys. Rev. Lett.* **107**, 056802 (2011).

[3] Ariando *et al*. Electronic phase separation at the $LaAlO_3/SrTiO_3$ interface. *Nature Commun.* **2**, 188 (2011).

[4] Li, L., Richter, C., Mannhart, J. & Ashoori, R. C. Coexistence of magnetic order and two-dimensional superconductivity at $LaAlO_3/SrTiO_3$ interfaces. *Nature Phys.* **7**, 762-766 (2011).

[5] Bert, J. A. *et al*. Direct imaging of the coexistence of ferromagnetism and superconductivity at the $LaAlO_3/SrTiO_3$ interface. *Nature Phys.* **7**, 767-771 (2011).

[6] Salman, Z. *et al.* Nature of weak magnetism in $SrTiO_3/LaAlO_3$ multilayers. *Phys. Rev. Lett.* **109**, 257207 (2012).

[7] Elfimov, I. S., Yunoki, S. & Sawatzky, G. A. Possible path to a new class of ferromagnetic and half-Metallic ferromagnetic materials. *Phys. Rev. Lett*. **89**, 216403 (2002).

[8] Pentcheva, R. & Pickett, W. E. Charge localization or itinerancy at $LaAlO_3$/$SrTiO_3$ interfaces: Hole polarons, oxygen vacancies, and mobile electrons. *Phys. Rev. B* **74**, 035112 (2006).

[9] Popović, Z., Satpathy, S. & Martin, R. M. Origin of the two-dimensional electron gas carrier density at the $LaAlO_3$ on $SrTiO_3$ interface. *Phys. Rev. Lett*. **101**, 256801 (2008).

[10] Pavlenko, N. *et al.* Magnetic and superconducting phases at the $LaAlO_3$/$SrTiO_3$ interface: The role of interfacial Ti 3d electrons. *Phys. Rev. B* **85**, 020407(R) (2012).

[11] Michaeli, K. Potter, A. C. & Lee, P. A. Superconducting and ferromagnetic phases in $SrTiO_3$/$LaAlO_3$ oxide interface structures: Possibility of finite momentum pairing. *Phys. Rev. Lett*. **108**, 117003 (2012).

[12] Hwang, H. Y. *et al*. Emergent phenomena at oxide interfaces. *Nature Mater.* **11**, 103-113 (2012).

[13] Ohtomo, A. & Hwang, H. Y. A high-mobility electron gas at the $LaAlO_3$/$SrTiO_3$ heterointerface. *Nature* **427**, 423-426 (2004).

[14] Reyren, N. *et al*. Superconducting interfaces between insulating oxides. *Science* **317**, 1196-1199 (2007).

[15] Kalisky, B. *et al.* Critical thickness for ferromagnetism in $LaAlO_3$/$SrTiO_3$ heterostructures. *Nature Commun.* **3**, 922 (2012).

[16] Gambardella, P. *et al*. Localized magnetic states of Fe, Co, and Ni impurities on alkali metal films. *Phys. Rev. Lett.* **88**, 047202 (2002).

[17] Fitzsimmons, M. R. *et al.* Upper limit to magnetism in $LaAlO_3/SrTiO_3$ heterostructures. *Phys. Rev. Lett*. **107**, 217201 (2011).

[18] Nakagawa, N., Hwang, H. Y. & Muller, D. A. Why some interfaces cannot be sharp. *Nature Mater*. **5**, 204-209 (2006).

[19] Sing, M. *et al*. Profiling the interface electron gas of $LaAlO_3/SrTiO_3$ heterostructures with hard x-ray photoelectron spectroscopy. *Phys. Rev. Lett*. **102**, 176805 (2009).

[20] Ikeno, H. *et al*. Multiplet calculations of $L_{2,3}$ x-ray absorption near-edge structures for 3*d* transition-metal compounds. *J. Phys.: Condens. Matter* **21**, 104208 (2009).

[21] The calculations were performed with $10Dq$ = 1.85 eV, Hubbard U_{dd} =1.5 eV and charge-transfer energy Δ= 1.2 eV for the Ti^{3+} state under O_h symmetry. Slater integrals were taken to be ~75% of the atomic values.

[22] Siemons, W. *et al*. Origin of charge density at $LaAlO_3$ on $SrTiO_3$ heterointerfaces: Possibility of intrinsic doping. *Phys. Rev. Lett.* **98**, 196802 (2007).

[23] Salluzzo, M. *et al*. Orbital reconstruction and the two-dimensional electron gas at the $LaAlO_3/SrTiO_3$ interface. *Phys. Rev. Lett.* **102**, 166804 (2009).

[24] Park, J. *et al*. Oxygen-vacancy-induced orbital reconstruction of Ti ions at the interface of $LaAlO_3/SrTiO_3$ heterostructures: A resonant soft-x-ray scattering study. *Phys. Rev. Lett*. **110**, 017401 (2013).

[25] Thiel, S. *et al*. Tunable quasi-two-dimensional electron gases in oxide heterostructures. *Science* **313**, 1942-1945 (2006).

[26] Bell, C. *et al*. Dominant mobility modulation by the electric field effect at the $LaAlO_3/SrTiO_3$ interface. *Phys. Rev. Lett.* **103**, 226802 (2009).

[27] Bell, C. *et al*. Thickness dependence of the mobility at the $LaAlO_3/SrTiO_3$ interface. *Appl. Phys. Lett*. **94**, 222111 (2009).

ACKNOWLEDGMENTS

We thank D. Nordlund, H. Ohldag, and D. Brehmer for experimental assistance in the spectroscopic measurements, and C. Chen, T. Devereaux, B. Kalisky, and K. Moler for useful discussions. Synchrotron studies were carried out at the SSRL, a Directorate of SLAC and an Office of Science User Facility operated for the U.S. DOE Office of Science by Stanford University. Y.W.X. acknowledges partial funding from the U.S. Air Force Office of Scientific Research (FAQSSO-10-1-0524). J.L., H.K.S., C.B., Y.H., and H.Y.H. acknowledge support by the Department of Energy, Office of Basic Energy Sciences, Materials Sciences and Engineering Division, under contract DE-AC02-76SF00515.

AUTHOR CONTRIBUTIONS

J.L., H.Y.H, and C.K. designed this project. J.L. and C.K. carried out the spectroscopy experiments. J.L., H.Y.H, and C.K analyzed the data and wrote this manuscript. Y.W.X., H.K.S., C.B., Y.H., and H.Y.H. grew and characterized the samples.

ADDITION INFORMATION

Supplementary information is available in the online version of the paper. Reprints and permissions information is available online at www.nature.com/reprints. Correspondence and requests for materials should be addressed to J.L.

COMPETING FINANCIAL INTERESTS

The authors declare that they have no competing financial interests.

FIGURE CAPTIONS

Figure 1| X-ray magnetic circular dichroism (XMCD) on a $LaAlO_3/SrTiO_3$ heterostructure. **a,** Schematic picture of the experimental configurations for the XMCD measurement. **b,** XMCD observed for the in-plane geometry, showing ferromagnetic Ti at T = 10 K (the displayed $\Delta\rho$ is the result of averaging 20 scans). The green and blue colored lines are the Ti^{3+} and Ti^{4+} XMCD spectra obtained from multiplet calculations, respectively. **c,** XMCD in the out-of-plane geometry ($\theta = 90^{o}$). All samples were zero-field cooled and measured in a constant applied field of +/- 0.2 T.

Figure 2| Characterizing the Ti valence state along the depth profile. a, X-ray absorption spectroscopy (XAS) results on LAO(0, 1, 2, 3, 5, 10, 15, and 25 UC)/STO heterostructures. The spectra are normalized at E = 457.1 eV. Two calculations represent the Ti^{3+} and Ti^{4+} states. The calculated Ti^{4+} spectrum has been multiplied by 100. The inset shows a schematic picture highlighting the probing depth and interfacial sensitivity via TEY. **b,** Two-dimensional map of XAS spectra around the Ti L_3-region. The white dashed lines indicates the energy position of the thinnest structure, LAO(1 UC)/STO. **c,** Enlarged t_{2g} level region. The black dashed line indicates the energy position of the t_{2g} level.

Figure 3| Spectroscopic diagram of the LAO/STO interface. a, Schematic energy diagrams of the crystal field splitting and 3*d* orbital degeneracy, showing the orbital reconstruction at the interface and local bonding change. O_h denotes the octahedral environment. **b,** The mixed valence Ti^{3+} and Ti^{4+} states at the interface.

Figure 4| Hybridization effects of Ti with neighboring oxygen. a, O *K*-edge XMCD in the LAO(3.3 UC)/STO heterostructure (T = 10 K, $\theta = 30^{o}$). The green shaded region indicates the Ti ferromagnetism at the t_{2g} level. **b,** O *K*-edge XLD for the LAO(3.3 UC)/STO heterostructure. The blue shaded regions indicate the Ti orbital states. **c,** Thickness dependence of the XAS spectra at O *K*-edge. The spectral change is pronounced above 3 UC in the vicinity of 542.5 eV (squares). Dashed lines denote the t_{2g} and e_g positions under Ti 3*d*-O 2*p* bonding. Triangles indicate the thickness variation of the XAS intensity.

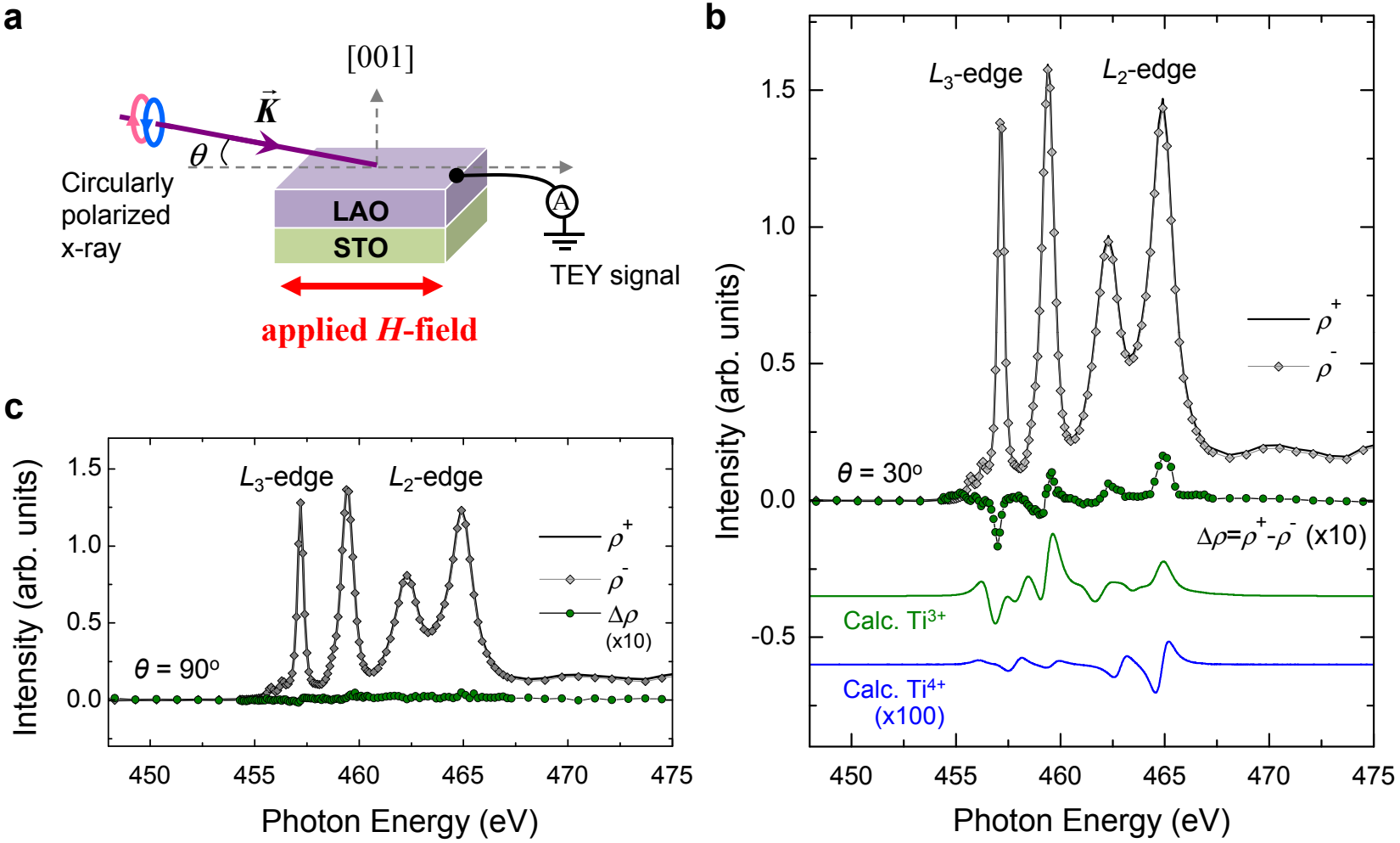

Figure 1: Lee *et al.*

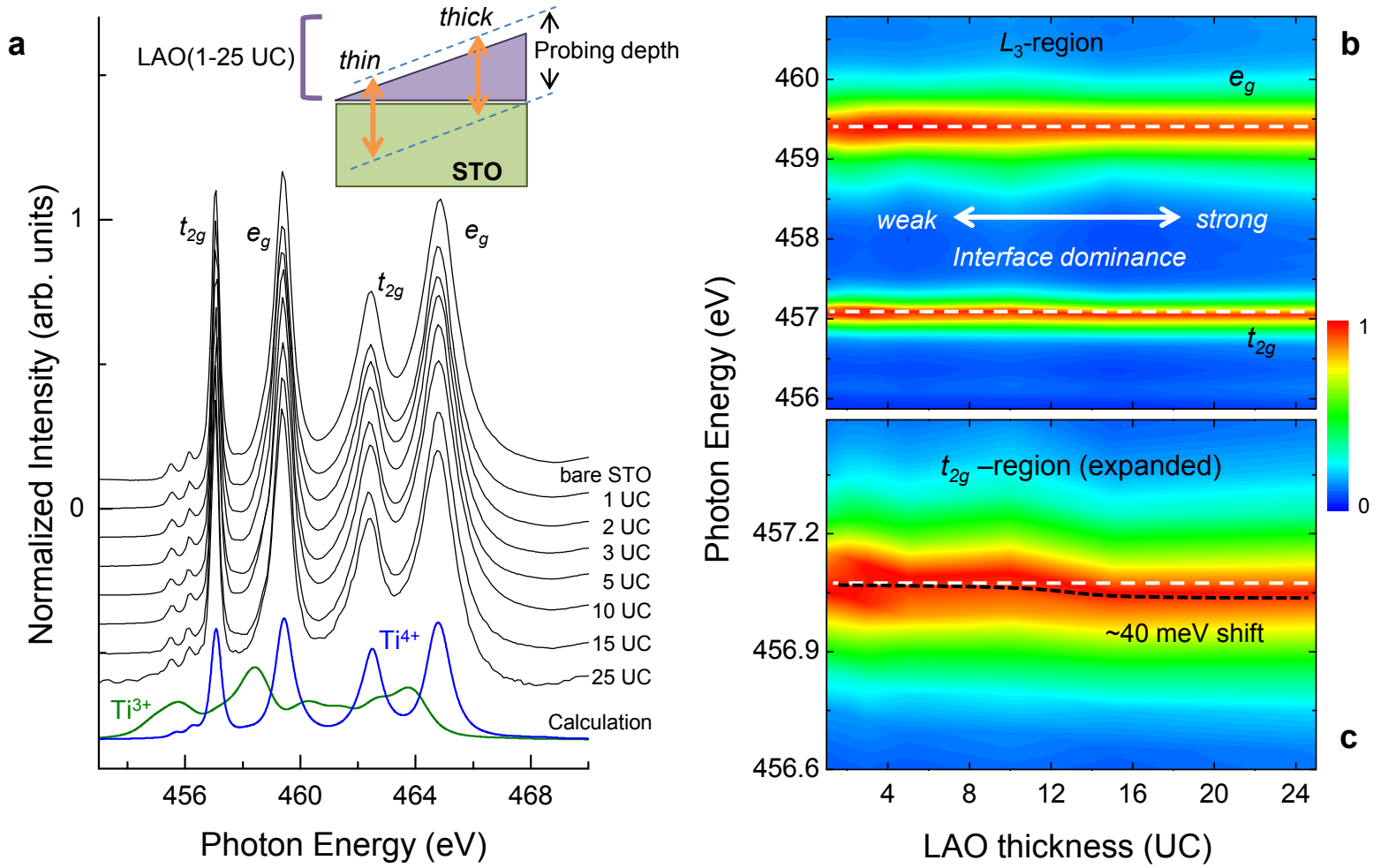

Figure 2: Lee *et al.*

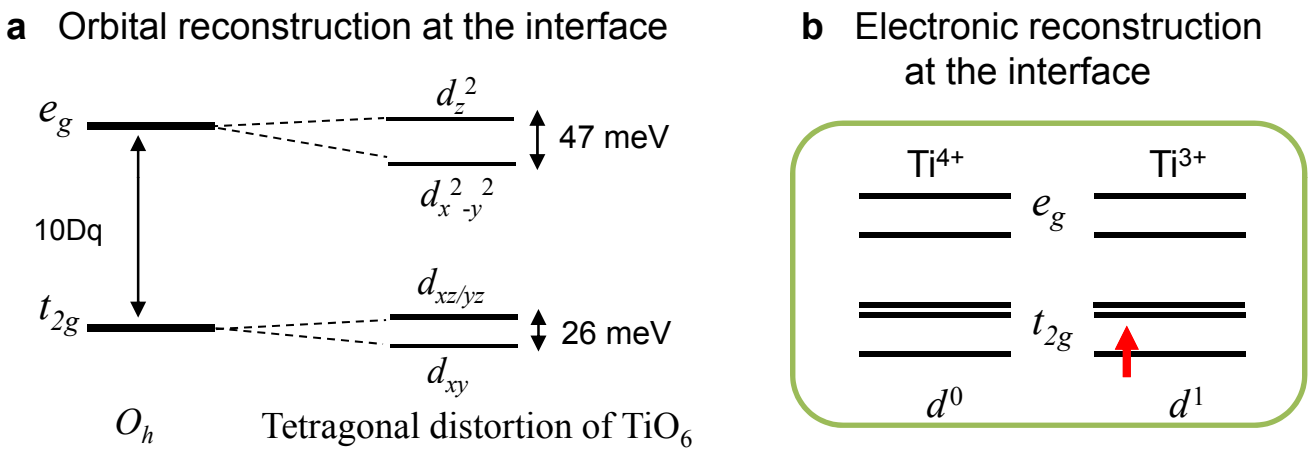

Figure 3: Lee *et al*.

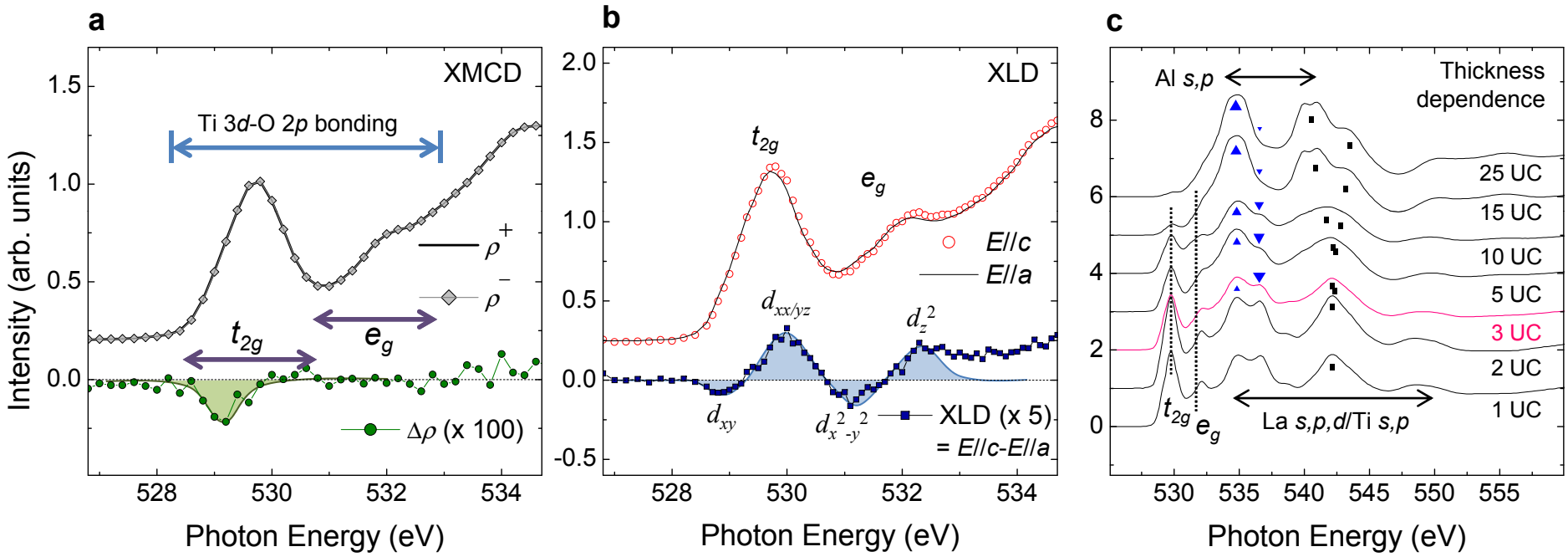

Figure 4: Lee *et al*.